

RESEARCH

Open Access



Polygonum multiflorum Stilbene Glycoside Oligomers induce the ferroptosis of triple negative breast cancer cells

Xiaomeng Lin^{1,2}, Hua Yang³, Tingting Cai⁴, Zhangshuo Yang^{1,2}, Siyun Niu^{5*} and Hui Jia^{6*}

Abstract

The quality control testing component and main active ingredient of *Polygonum multiflorum* Thunb. (*P. multiflorum*), known as trans-2,3,5,4'-tetrahydroxystilbene 2-O- β -D-glucopyranoside (TSG), exhibits diverse biological activities. In this study, we report, for the first time, the potent ability of TSG to induce ferroptosis in triple negative breast cancer (TNBC) cell lines and to inhibit the proliferation of TNBC cells. Treatment with TSG triggers the production of lipid peroxides, 4-hydroxynonenal (4-HNE), and reactive oxygen species (ROS) in TNBC cells, indicating the induction of ferroptosis. Both in vivo and in vitro experiments confirmed the inhibitory effects of TSG on TNBC cell proliferation and metastasis. Furthermore, we investigated the effects of other stilbene glycoside oligomers, alongside TSG, on TNBC cell lines. These compounds also demonstrated the ability to induce ferroptosis and suppress TNBC cells' proliferation and metastasis. These findings suggest that the induction of ferroptosis by TSG and related compounds could potentially serve as a promising therapeutic strategy for TNBC treatment.

Keywords *Polygonum multiflorum* Thunb, Trans 2,3,5,4'-tetrahydroxystilbene 2-O- β -D glucopyranoside, Triple negative breast cancer

*Correspondence:

Siyun Niu

nsy1688@163.com

Hui Jia

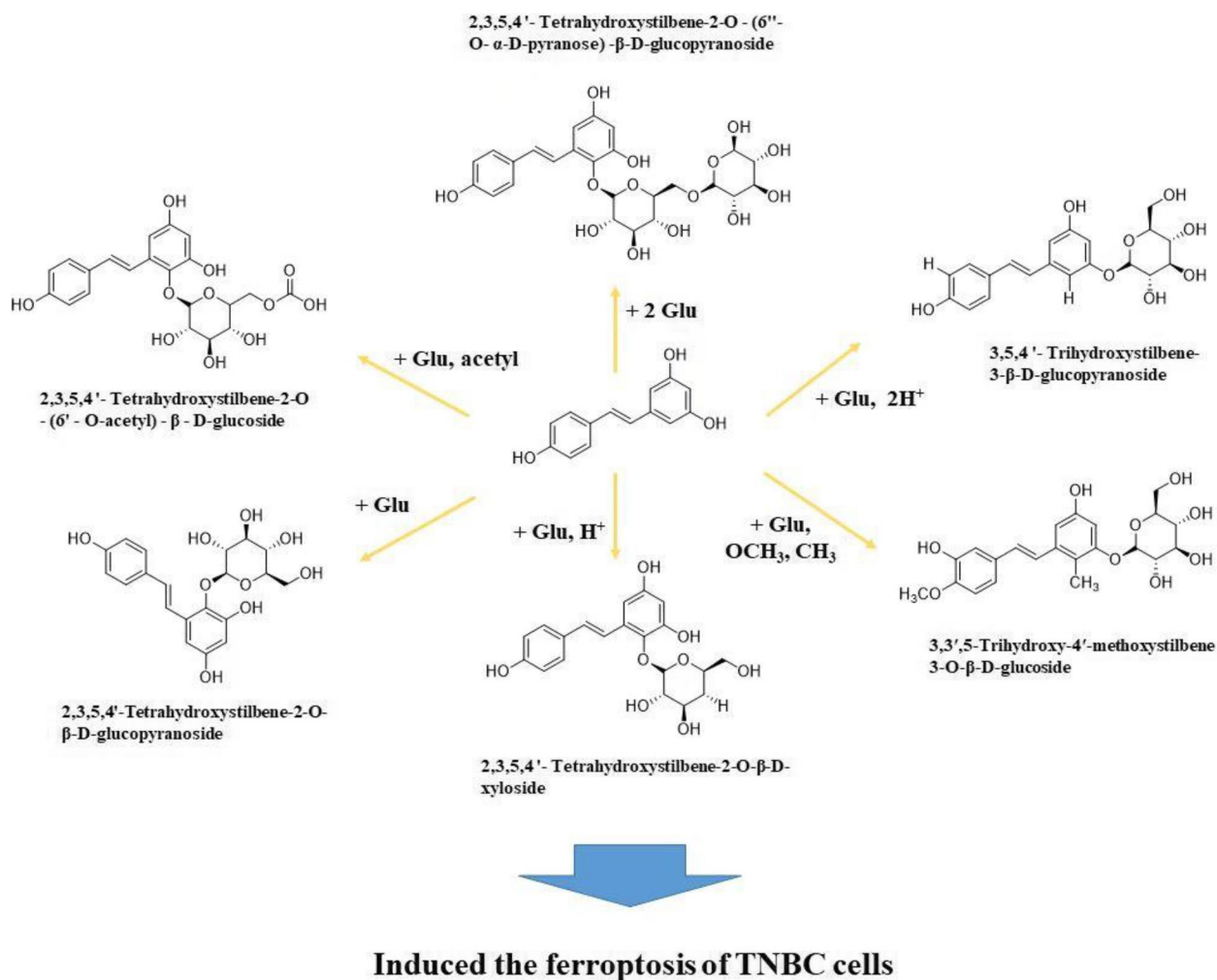
huijia412413@symc.edu.cn

Full list of author information is available at the end of the article



© The Author(s) 2025. **Open Access** This article is licensed under a Creative Commons Attribution-NonCommercial-NoDerivatives 4.0 International License, which permits any non-commercial use, sharing, distribution and reproduction in any medium or format, as long as you give appropriate credit to the original author(s) and the source, provide a link to the Creative Commons licence, and indicate if you modified the licensed material. You do not have permission under this licence to share adapted material derived from this article or parts of it. The images or other third party material in this article are included in the article's Creative Commons licence, unless indicated otherwise in a credit line to the material. If material is not included in the article's Creative Commons licence and your intended use is not permitted by statutory regulation or exceeds the permitted use, you will need to obtain permission directly from the copyright holder. To view a copy of this licence, visit <http://creativecommons.org/licenses/by-nc-nd/4.0/>.

Graphical Abstract



Introduction

Polygonum multiflorum Thunb. (*P. multiflorum*), a climbing vine plant belonging to the Polygonaceae family, holds the significant traditional significance in China as a renowned rug-food homologous natural product [1]. Its roots have diverse activities and applications. Scientific evidence suggests that *P. multiflorum* contains stilbene glycoside dimers, particularly the trans-2,3,5,4'-tetrahydroxystilbene 2-O- β -D-glucopyranoside (TSG) is considered as the active components of *P. multiflorum* [2, 3]. While existing research on *P. multiflorum* were mainly extensively studied the effects of stilbene glycoside dimers like trans-2,3,5,4'-tetrahydroxystilbene 2-O- β -D-glucopyranoside (TSG) primarily focused on cardiovascular and neurological diseases, and limited

research has explored their potential antitumor properties [4]. Molecular studies have revealed that TSG can inhibit several signaling pathways crucial for tumor progression and drug resistance [5, 6]. These pathways include: PI3K /AKT, TGF β /Smads and MAPK signalling pathway [4–6]. Given the pivotal role of these pathways in tumor onset and development, the antitumor potential of TSG and related compounds deserves further investigation.

Triple-negative breast cancer (TNBC) remains the most aggressive and common form of gynecological malignancy, posing significant risks to women's health [7]. Recent studies have highlighted TNBC's heterogeneity and the need for further classification into distinct subtypes [8]. Currently, only patients with germline

BRCA mutations are considered sensitive to olaparib [9]. Therefore, it is crucial to investigate novel and effective therapeutic strategies targeting a broader spectrum of TNBC cases.

Ferroptosis, a unique form of programmed cell death different from apoptosis, necrosis, or pyroptosis [10], has emerged as a promising potential therapeutic target for treating breast cancer. Studies have shown its critical role in suppressing breast tumor growth by modulating various cancerous properties [11]. Furthermore, research is focusing on developing agents or drugs that induce ferroptosis to combat breast cancer cells [11]. These findings suggest that targeting ferroptosis may hold significant promise as a novel therapeutic approach for treating TNBC. In the presence, our results, for the first time, demonstrated that several compounds, including TSG and other kinds of stilbene glycoside dimers, can trigger ferroptosis in TNBC cells. These findings have highlighted the role of TSG in suppressing TNBC breast cancer growth by inducing ferroptosis and cell cycle arrest. Our study not only sheds new light on the anti-tumor effects of *P. multiflorum* but also suggests that targeting ferroptosis may hold promise as a therapeutic strategy for treating TNBC.

Materials and methods

Cell lines and agents

The cell lines used in this study included MDA-MB-231, HCC-1937, and MDA-MB-436, which were described in previous publications [9]. Additionally, we purchased 4T1, BT20, and MDA-MB-453 cell lines from the Type Culture Collection of the Chinese Academy of Sciences (Shanghai, China). These cell lines were cultured in Dulbecco's Modified Eagle Medium (DMEM) supplemented with 10% fetal bovine serum (FBS). The agents used in this study included six kinds of stilbene glycosides from *Polygonum multiflorum*: compound 1 (2,3,5,4'-tetrahydroxystilbene-2-O-(6''-O- α -D-pyranose)- β -D-glucopyranoside), compound 2 (2,3,5,4'-tetrahydroxystilbene-2-O- β -D-xyloside), compound 3 (2,3,5,4'-tetrahydroxystilbene-2-O-(6'-O-acetyl)- β -D-glucoside), TSG (compound 4), compound 5 (3,3',5-trihydroxy-4'-methoxystilbene-3-O- β -D-glucoside), and compound 6 (3,5,4'-trihydroxystilbene-3- β -D-glucopyranoside). Of these, TSG (compound 4), compound 5, and compound 6 were purchased from Selleck Corporation (Houston, Texas, USA), while compounds 1 to 3 were isolated by our research team. *Polygonum multiflorum* medicinal herb was extracted with 70% ethanol reflux for 3 times, each time for 1 h. The extracted solutions were combined, left at room temperature, filtered, and the ethanol was recovered and concentrated into a paste. Dissolve the extract in water, extract with dichloromethane to remove impurities, pass through

DM-8 macroporous resin, and remove with 95%, 55%, 40%, and 25% concentration ethanol and water, respectively. The 20% ethanol extract was eluted by gel column chromatography Sephadex LH-20 to obtain compounds 1–3. In addition to these natural product monomer molecules, this study also used three tool drugs: sorafenib (Selleck Corporation, Houston, Texas, USA), ferostatin (Selleck Corporation, Houston, Texas, USA), and N-Acetyl cysteine (NAC) (Selleck Corporation, Houston, Texas, USA).

In our cellular experiments, we accurately measured out the correct dosages of these drugs using a high-precision balance with a precision of 1 in 100,000. Then, the drugs were dissolved in Dimethyl sulfoxide (DMSO) before diluting them with DMEM without FBS. The dosages used for TSG were 5 μ mol/L, 10 μ mol/L, and 20 μ mol/L. In our animal experiments, a similar approach using a high-precision balance were performed to measure out the correct dosages of drugs. These drugs were diluted in physiological saline before administering them via injection. The dosages used for TSG were 5 mg/kg, 10 mg/kg, and 20 mg/kg in animal experiments.

Quantitative polymerase chain reaction (qPCR)

For our cell-based qPCR experiments, the TNBC cell lines such as MDA-MB-231, HCC-1937, and MDA-MB-436, 4T1, BT20, and MDA-MB-453 were cultured these cells and treated them with the indicated concentrations of compounds. Then, we extracted total RNA from the cell samples using a method similar to that used for tissue analysis (described below). Next, the RNA samples were reverse transcribed into cDNA using a SuperScriptTM IV VILOTM Master Mix according to the manufacturer's instructions and performed on an ABI-7500 Real-Time Fluorescence Quantitative PCR Instrument Program (ABI Corporation, USA).

For our tumor tissue analysis, MDA-MB-231 cells were cultured in nude mice to form subcutaneous tumors. The mice were received with TSG via oral administration and the tumor tissues were harvested. After gently rinsing the subcutaneous tumor tissue with pre-sterilized DEPC-treated deionized water, we cut the tumor tissue into small pieces using sterilized ophthalmic shears and ophthalmic forceps. Next, these small chunks of tumor tissue were mixed with RNA Later and then crushed. The tumor tissue samples were centrifuged at 12000 rpm at 4 °C for over 15 min to separate out the supernatant fraction from the previous step. The RNA samples were extracted from the supernatant fraction using gDNA Eliminator columns, RLT RNeasy centrifugal adsorbent columns, Buffer RW1, and DEPC-treated deionized water, respectively. After reverse transcription, qPCR experiments were performed by using Power SYBR

Green 1-Step Kit with Ki67 (an indicator of cell proliferation) as the target gene and GAPDH as a reference. The primers used for their amplification were obtained from the Origin website. The expression of Ki67 was calculated based on the ratio of Ki67 CT values in qPCR experiments to the CT values of GAPDH.

Cell survival examination

Firstly, to examine the antitumor activation of compounds 1 to 6 on TNBC cells, we first performed CCK-8 assays using a method similar to that described previously. The TNBC cells were cultured and seeded in 96-well plates at an initial concentration of 8000 cells per well. Then, the cells were treated with compounds 1 to 6 (at a concentration of 20 $\mu\text{mol/L}$) for 48 h. Next, we conducted cell viability assays using CCK-8 kits (Dojindo Laboratories, Japan) according to the manufacturer's instructions and the methods described in our previous publication [9]. The results were shown as heatmaps based on the inhibitory rates.

Secondly, we performed colony formation assays by culturing MDA-MB-231 cells in triplicate at 2000 cells per well in six 6-well plates (Corning Corporation, USA) [12]. After allowing the cells to adhere overnight, we continuously cultured them for 10–14 days until colonies of cells formed and were observable. To fix the colonies, we used 4% paraformaldehyde solution for 15 min and then stained them with crystal violet solution for 30 min at room temperature. We washed them three times before scanning them with an HP Scanjet (HP Corporation, USA). To quantify the images obtained from the assay, we used image J software (National Institutes of Health, Bethesda, Maryland, USA) according to our previous publication. Briefly, we converted the images into pure black-and-white format before analyzing them.

Thirdly, to assess the cell migration and invasion abilities of MDA-MB-231 cells treated with TSG, we performed two assays [12]. For the cell migration assay, we scratched the monolayer of MDA-MB-231 cells mechanically using a 200- μL pipette tip to create gaps for the cells to migrate through. We then washed away any debris with PBS and treated the cells with TSG in DMEM without FBS. We obtained images of the cells at both the 0 h (time point) and 12 h markings, documenting the distances between each gap in the cell monolayer to quantify the degree of migration. To perform the cell invasion assay, we prepared MDA-MB-231 cells treated with TSG and then added liquid Matrigel onto the upper surface of transwell chambers (BD Biosciences, USA). We added single-cell suspensions (MDA-MB-231 cells diluted in DMEM without FBS) into the upper surface of the transwell chambers (about 10,000 cells per well).

After adding DMEM containing 10% FBS to the transwell chambers, we incubated them for 12 h at 37 °C. We fixed the invaded cells using 4% paraformaldehyde and stained them with crystal violet solution (5% w/v). To quantify the degree of cell invasion, we obtained images of transwell chambers using phase-contrast microscopy and counted the number of invaded cells.

Cellular ferroptosis measurement

Two assays (lipid peroxidation and ROS levels) were performed to measure the effect of TSG inducing ferroptosis in TNBC cells treated with compound 1–6 [10, 11]. Firstly, we used a 10 $\mu\text{mol/L}$ dose of C11-BODIPY dye (Cat. No.: D3861; Thermo Fisher Scientific, Waltham, MA, USA) and flow cytometry analysis (FACS Canto II; BD Biosciences, USA) to assess lipid peroxidation levels. Secondly, we measured the ROS level in TNBC cells using a 25 $\mu\text{mol/L}$ dose of carboxy-H₂DCFDA (88–5930-74; Invitrogen, Thermo Fisher Scientific, Waltham, MA, USA) and flow cytometry analysis (the 488 nm wavelength excitation and the 525 nm wavelength emission) (FACS Canto II; BD Biosciences, USA). In addition to these analyses, glutathione in MDA-MB-231 cells was also detected. MDA-MB-231 cells were cultured and treated with TSG at a series of concentration gradients for 24 h, followed by detection using a glutathione assay kit (Cat. No.: CS0260; Sigma-Aldrich, Merck Corporation, Darmstadt, Germany). At this time, 5,5'-dithiobis (2-nitrobenzoic acid) in the reagent kit can react with glutathione (GSH) to produce 2-nitro-5-mercaptobenzoic acid and glutathione disulfide (GSSG). Furthermore, the content of glutathione in the sample was determined by measuring the absorbance value at a wavelength of 412 nm.

Cell cycle analysis

The TNBC cells were cultured and transfected with vectors before being prepared as single-cell suspensions. The single-cell suspensions were then seeded into 6-well plates (1×10^6 cells per well). When the cells had spread over almost all of the bottom of the plate (essentially covering 80–90% of the cell area), they were treated with different concentrations of TSG. To analyze the cell cycle, we fixed the cells in 75% ethanol for more than 18 h at 4 °C before washing them twice with PBS and incubating them with RNase A (0.2 mg/mL) in PBS. Propidium iodide was then added to the cell suspension, and we analyzed the samples using a FACS Calibur Flow Cytometer (Becton Dickinson, Franklin Lakes, NJ, USA) [13].

The *in vivo* subcutaneous tumor model

The Experimental Animal Ethics Committee of the Affiliated Hospital of Hebei University approved and

reviewed the breeding and use of experimental animals, as well as the study protocol, including experimental procedures and animal welfare measures. In this study, we used the MDA-MB-231 cells, which were cultured before being subcutaneously injected into six-week-old female nude mice (the thymus-deficient BalB/c immunodeficient mice) from Vital River Laboratory Animal Technology (Beijing) in an SPF condition. During the entire process of animal experiments, the animals were randomized or blinded to ensure objectivity in the results: Ensure that the age of the experimental animals is exactly the same, and at the same time, weigh the experimental animals to select those with similar body weights. At the same time, number the animals and group them according to a random number table.

Each experimental animal is inoculated with cells once, forming a subcutaneous tumor tissue. Each group has $n=10$. Each animal received a 5×10^6 amount of MDA-MB-231 cells, and five or six days after injection, we administered TSG orally to the mice at doses of 5, 10, and 20 mg/kg in a 15-dosing regimen every three days. After all animal experiments, the tumor size were measured by using calipers (longest diameter \times shortest diameter \times shortest diameter / 2) [14]. At the end-point, the subcutaneous tumor tissues were separated from the animals and weighed by using a precision balance. When the animals and tumor tissues were collected at the end-point of the experiment, the procedure of killing the animals was carried out in accordance with the principle of euthanasia (under the premise of ensuring that the animals were unconscious): the animals were anesthetized by inhalation anesthesia (anesthesia was rapid, thorough, convenient and) method (inhalation anesthetic was isoflurane, the concentration was 1.5% v/v), and the animals were euthanised killed immediately after complete anesthesia.

Moreover, we prepared the tumor tissues as paraffin sections for pathological analysis: we mounted the paraffin Sects. (3 mm) on slides and dried them in a 60 °C oven. We then placed the slides on a Leica BondMax Immunostainer. We optimized the dilution of antibodies with a predetermined staining protocol: 1:1000 for Ki67 and 1:500 for 4-HNE. Using a Lipid Peroxidation (4-HNE) Assay Kit (ab238538; Abcam, UK), we performed slides by DAB methods and obtained images. All antibodies were purchased from Abcam Corporation, UK. The immunohistochemical results of 4-HNE and Ki67 were quantitatively analyze using Image J software. At this point, the images were imported into Image J software, then identify and circle the yellow brown stained areas, and perform quantitative analysis

based on the staining depth of the total area of the stained positive areas.

Western blot

The MDA-MB-436 cells were treated with the indicated concentrations (5, 10, and 20 $\mu\text{mol/L}$) of TSG for 24 h. After TSG treatment, the cells were harvested for western blot. The experiment was carried out according to the protocol of conventional western blot: prepare samples of total cell protein, configure SDS-PAGE gel (compression gel 5%; separation gel 12.5%) and carry out SDS-PAGE electrophoresis (compression gel 80 V electrophoresis for 30 min; separation gel 120 V electrophoresis for 1.5 h), and then use a semi dry membrane converter at 15 V. Afterwards, 10% (w/v) skim milk powder blocking solution was prepared using TBST buffer to block the PVDF membrane. Preparing 5% (w/v) skim milk powder with TBST buffer to dilute antibodies, and PVDF membranes were incubated with antibodies against SLC7A1 (Cat, No.: ab153920, Abcam, Cambridge, UK), p53 (Cat, No.: ab26, Abcam, Cambridge, UK), p21 (Cat, No.: ab109520, Abcam, Cambridge, UK), GPX4 (Cat, No.: ab125066, Abcam, Cambridge, UK), and β - actin (Cat, No.: ab8226, Abcam, Cambridge, UK). Chemiluminescence method was next used.

Ethics statement in the presence work

In this study, human-related materials were only cell lines purchased from a Typical Biomaterials Conservation Center of Chinese Government. To ensure that all animal experiments were conducted ethically and following established protocols, the Animal Ethics Committee of Affiliated Hospital of Hebei University reviewed and approved the breeding and use of experimental animals, as well as the experimental designs and methods (approval ID: IACUC-2021XG020). All animal experiments were performed in accordance with the UK Animals (Scientific Procedures) Act of 1986 and associated guidelines.

Statistical analysis

In this study, we performed all in vitro experiments in triplicate to ensure statistical significance and accuracy of results. We used chi-square analysis, two-tailed Student's t test, or one-way analysis of variance to assess differences between variables. All statistical analyses were performed using either SPSS 13.0 or Prism 6 (GraphPad), and all data is presented as the mean \pm standard deviations. In all assays, we considered $p < 0.05$ as statistically significant.

Results

TSG induced the ferroptosis of TNBC cell line MDA-MB-231
 Firstly, to evaluate the effect of TSG on ferroptosis in TNBC cells, we performed multiple assays to explore the

lipid peroxidation and ROS promotion effects. As shown in Fig. 1A, compared with the control group, treatment of TSG dose-dependently increased lipid peroxidation levels in MDA-MB-231 cell line. Specifically, the relative fold

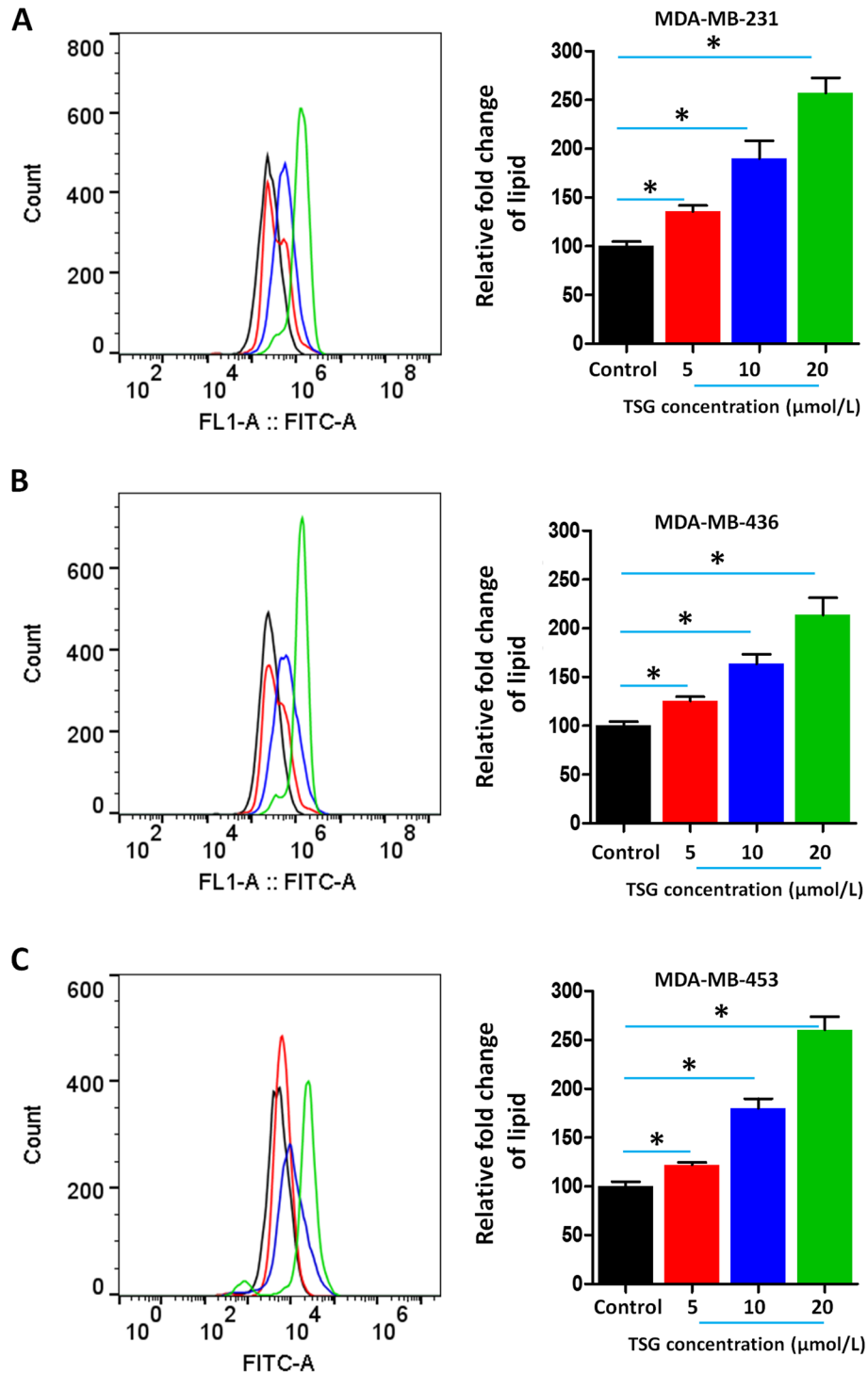


Fig. 1 TSG induced the lipid peroxidation of TNBC cells

change of lipid peroxidation increased from 100.00 ± 9.33 (control group) to 132.94 ± 6.79 (TSG 5 $\mu\text{mol/L}$ group), 190.35 ± 31.53 (TSG 10 $\mu\text{mol/L}$ group), or 257.07 ± 26.74 (TSG 20 $\mu\text{mol/L}$ group) respectively.

Next, according to the results in Fig. 2A, treatment with TSG increased ROS levels in MDA-MB-231 cells in a dose-dependent manner. Compared with the control group (100.00 ± 7.90), which had a relative fold change

of ROS of 1, the relative fold change of ROS increased to 165.50 ± 15.74 (TSG 5 $\mu\text{mol/L}$ group), 256.83 ± 27.949 (TSG 10 $\mu\text{mol/L}$ group), or 357.18 ± 26.66 (TSG 20 $\mu\text{mol/L}$ group) respectively. These results suggest that TSG could induce ferroptosis in MDA-MB-231 TNBC cells.

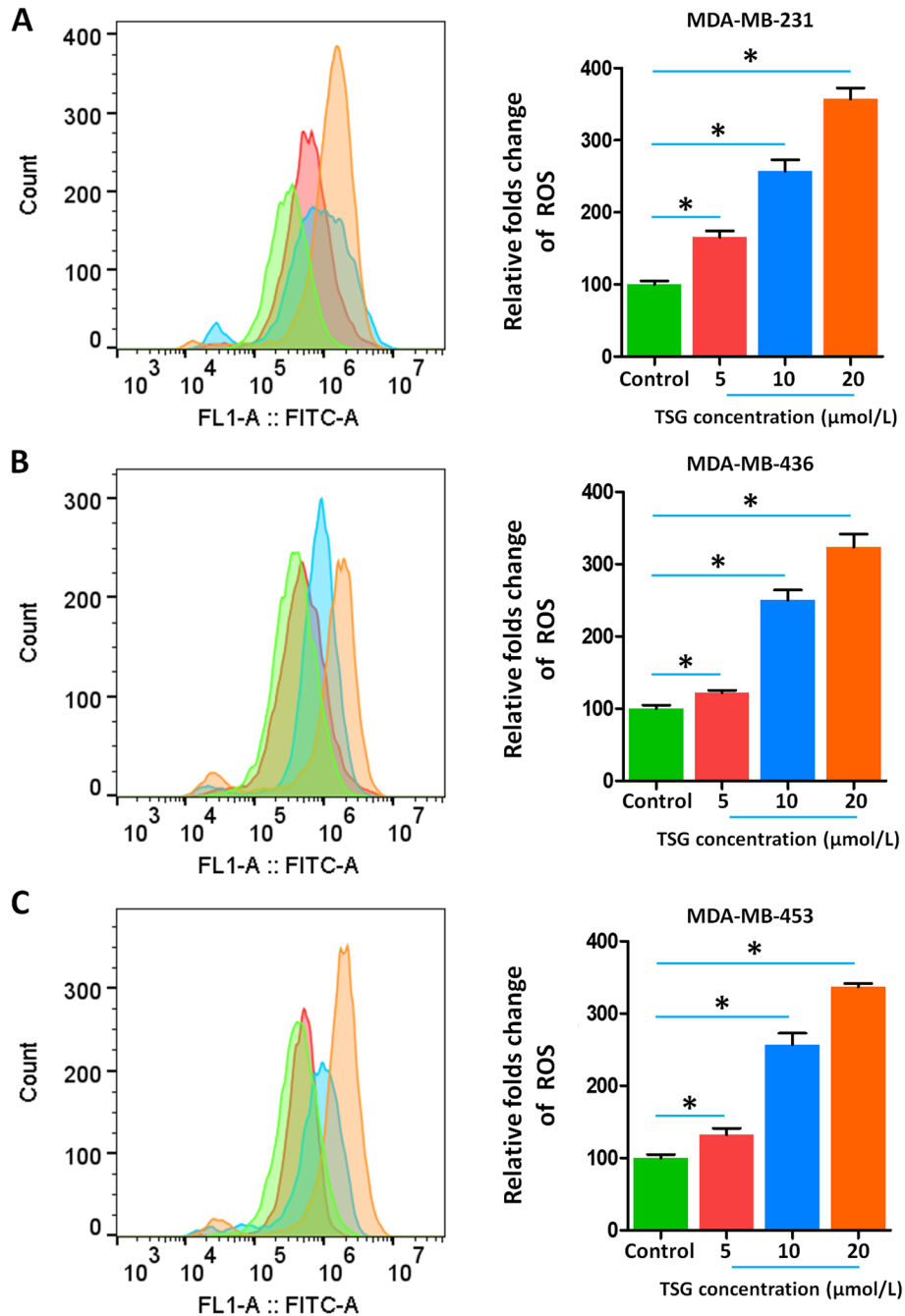


Fig. 2 TSG induced the ROS accumulation in TNBC cells

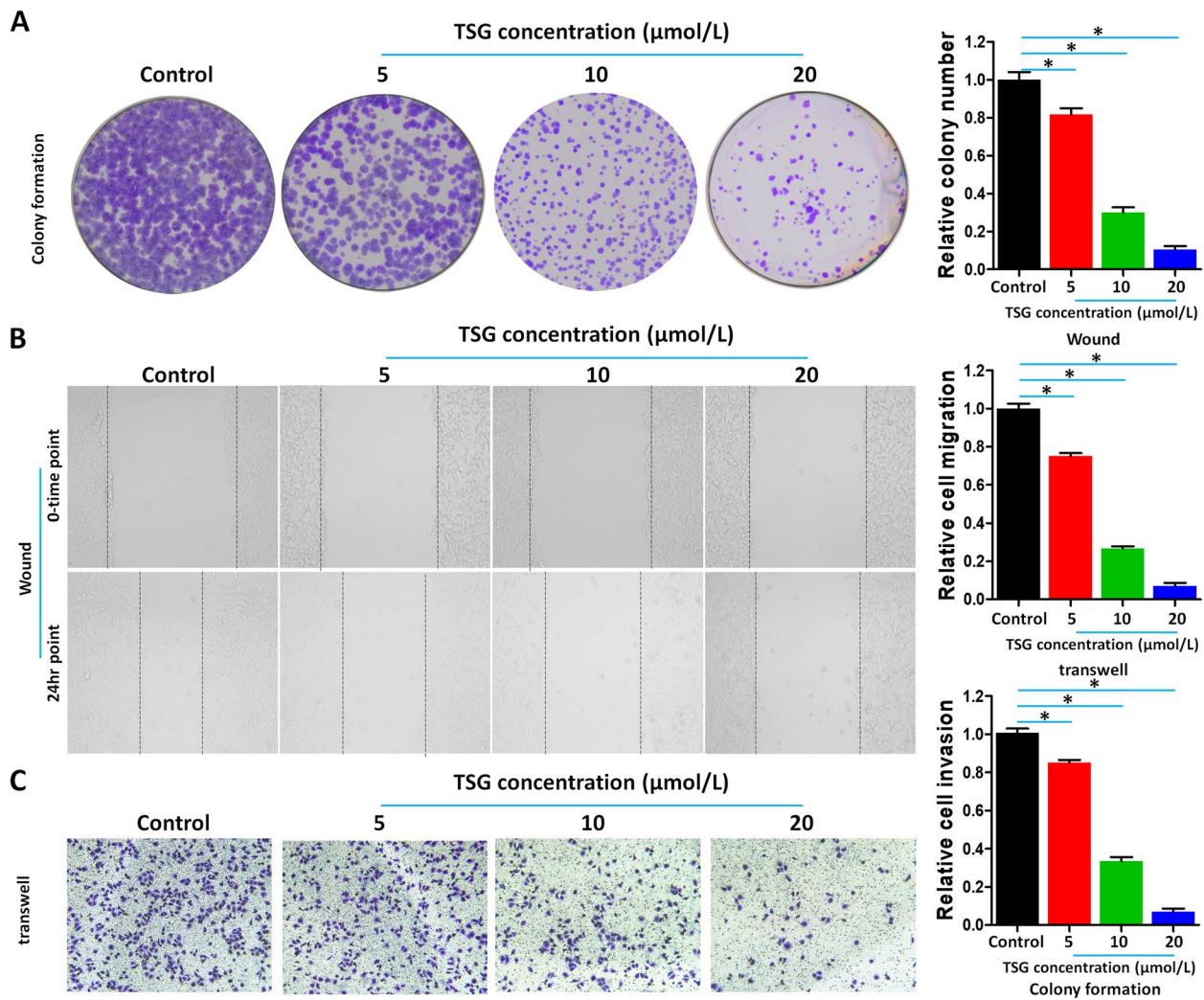


Fig. 3 TSG treatment inhibited the in vitro survival, migration and invasion of TNBC cell line MDA-MB-231

TSG demonstrates multifaceted antitumour activity on TNBC cell line MDA-MB-231

To further evaluate the antitumor effect of TSG on TNBC cells, we performed multiple assays to assess cell survival. As shown in Fig. 3A, treatment of TSG dose-dependently inhibited the colony formation of MDA-MB-231 cell line. Specifically, the inhibitory rate of TSG on MDA-MB-231’s colony formation increased from 16.44 ± 6.22% (TSG 5 μmol/L group) to 69.8 ± 4.52%, and finally to 90.6 ± 2.29%. These results suggest that TSG could have antitumor effects on MDA-MB-231 TNBC cells.

Next, to evaluate the in vitro migration and invasion of MDA-MB-231 cells, we performed cell scratching / wound-healing assay and transwell assays. As shown in Fig. 3B, treatment of TSG dose-dependently inhibited the in vitro migration of MDA-MB-231 cell line. Specifically, the inhibitory rate of TSG on MDA-MB-231’s in vitro migration increased from 25.00 ± 2.65% (TSG 5 μmol/L

group) to 73.33 ± 2.08%, and finally to 92.90 ± 1.18%. Similarly, treatment of TSG dose-dependently inhibited the in vitro invasion of MDA-MB-231 cells, with inhibitory rates of 15.27 ± 2.32% (TSG 5 μmol/L group), 66.93 ± 1.60%, and 92.60 ± 3.12%. These results suggest that TSG could have antimetastatic effects on MDA-MB-231 TNBC cells.

To further investigate the effect of TSG on MDA-MB-231 cell cycle progression, we conducted flow cytometry analysis. As shown in Fig. 4, treatment of TSG arrested the cell cycle progress of MDA-MB-231 cells at G2/M phase. Specifically, the proportion of MDA-MB-231 cells at G2/M phase increased from 48.19 ± 2.68% in the control group to 57.77 ± 1.06%, 61.14 ± 0.31%, and finally to 64.83 ± 2.14% in the TSG 5 μmol/L, 10 μmol/L, and 20 μmol/L groups respectively. Therefore, TSG demonstrates multifaceted antitumor activity on MDA-MB-231 TNBC cell line.

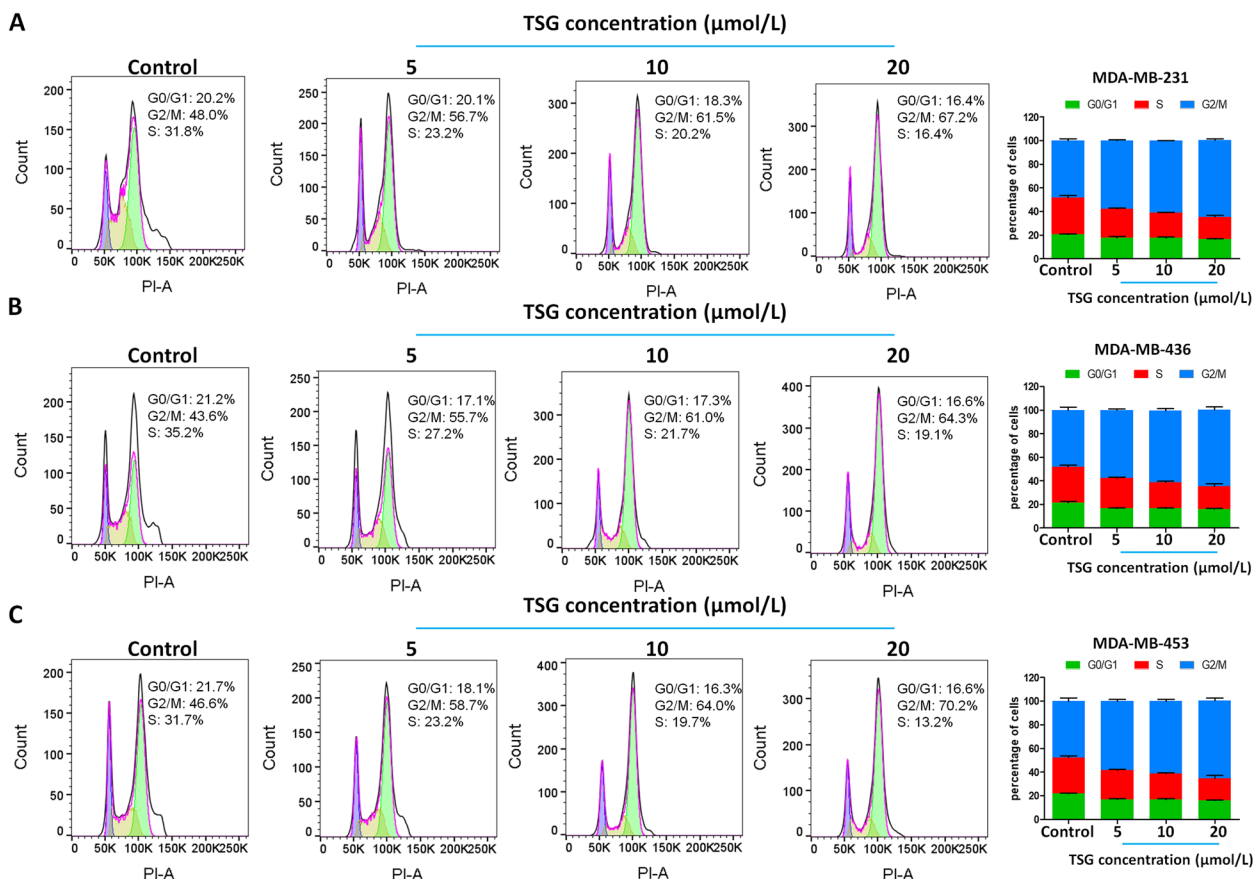


Fig. 4 TSG treatment induced the G2/M arrest of TNBC cells' cell-cycle progress

TSG induced the ferroptosis and demonstrates antitumour activity on TNBC cell lines

We examined the effect of TSG on other TNBC cells (MDA-MB-436 and MDA-MB-453) in addition to MDA-MB-231. As shown in Fig. 1B and C, treatment of TSG induced ferroptosis of MDA-MB-436 and MDA-MB-453 cells in a dose-dependent manner: the lipid peroxidation level of MDA-MB-436 cells increased from $100 \pm 6.53\%$ (control group) to $125.50 \pm 7.78\%$ (TSG 5 μmol/L group), $162.77 \pm 21.38\%$ (TSG 10 μmol/L group), or $213.73 \pm 30.43\%$ (TSG 20 μmol/L group); the lipid peroxidation level of MDA-MB-453 increased from $100 \pm 9.12\%$ (control group) to $122.94 \pm 3.21\%$ (TSG 5 μmol/L group), $179.78 \pm 17.57\%$ (TSG 10 μmol/L group), or $260.37 \pm 23.52\%$ (TSG 20 μmol/L group); respectively.

Moreover, as shown in Fig. 2B and C, the ROS level of MDA-MB-436 cells also increased from $100.00 \pm 7.61\%$ (control group) to $123.54 \pm 6.758\%$ (TSG 5 μmol/L group), $252.15 \pm 22.05\%$ (TSG 10 μmol/L group), or $313.13 \pm 2.91\%$ (TSG 20 μmol/L group); the ROS level of MDA-MB-453 also increased from $100.00 \pm 9.14\%$ (control group) to $131.34 \pm 14.45\%$ (TSG 5 μmol/L

group), $266.05 \pm 42.96\%$ (TSG 10 μmol/L group), or $334.31 \pm 6.27\%$ (TSG 20 μmol/L group); respectively.

We also observed that the treatment of TSG led to cell cycle arrest at G2/M phase, as shown in Fig. 4B and C. Specifically, the proportion of MDA-MB-436 cells at G2/M phase increased from $48.27 \pm 4.46\%$ (control group) to $56.68 \pm 2.51\%$ (TSG 5 μmol/L group), $60.76 \pm 3.02\%$ (TSG 10 μmol/L group), and $64.84 \pm 4.11\%$ (TSG 20 μmol/L group); the proportion of MDA-MB-453 cells at G2/M phase increased from $47.22 \pm 3.95\%$ (TSG 5 μmol/L group) to $59.13 \pm 2.17\%$ (TSG 5 μmol/L group), $61.27 \pm 2.73\%$ (TSG 10 μmol/L group), and $66.33 \pm 3.60\%$ (TSG 20 μmol/L group); respectively. Therefore, TSG demonstrates multifaceted antitumor activity on TNBC cell lines.

TSG inhibited the in vivo growth of TNBC cell line MDA-MB-231 and induced the ferroptosis in nude mice

To further examine the antitumor activity of TSG on TNBC cells, a nude mouse subcutaneous tumor model was used to investigate the ferroptosis of MDA-MB-231 cells. As shown in the Fig. 5, MDA-MB-231 cells formed subcutaneous tumors in the nude mice. We found that

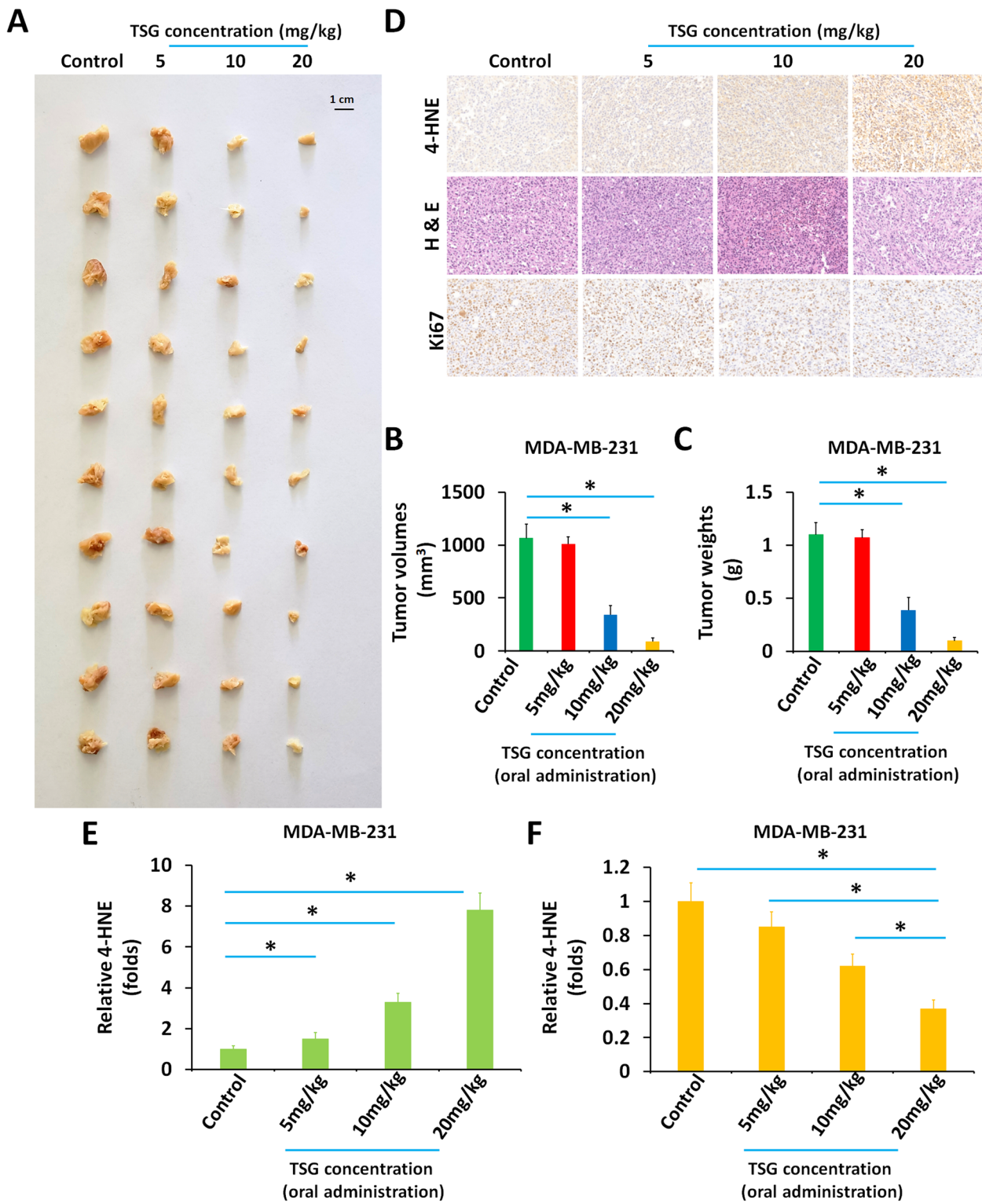


Fig. 5 TSG inhibited the in vivo growth of MDA-MB-231 cells in a nude mice model

treatment of TSG inhibited the growth of MDA-MB-231 cells in a dose-dependent manner (Fig. 5A-C). Additionally, we performed hematoxylin and eosin (H&E) staining, Ki67 staining, and lipid peroxide 4-hydroxy-2-nonenal (4-HNE) staining to confirm the results of the in vivo assay (Fig. 5D-F). The H&E staining images confirmed that TSG treatment effectively inhibited the growth of MDA-MB-231 tumors (Fig. 5D-F). Furthermore, the Ki67 staining assay showed that TSG decreased the expression of Ki67 (a proliferation marker for cancerous cells) in MDA-MB-231 tumor tissues. Moreover, we found that TSG treatment increased 4-HNE levels in MDA-MB-231 tissues, indicating that TSG induced ferroptosis of MDA-MB-231 cells in subcutaneous tumor tissues. In conclusion, our results suggest that TSG inhibits the growth of TNBC cell line MDA-MB-231 in nude mice.

The effect of Polygonum multiflorum Stilbene Glycoside Oligomers on several kinds of TNBC cells

To further verify the effectiveness of Polygonum multiflorum Stilbene Glycoside Oligomers against TNBC, we used other cell types and compounds in addition to TSG. As shown in Fig. 6, a 20 μmol/L concentration of Compound 1, Compound 2, Compound 3, Compound 5, and Compound 6 all effectively inhibited

the survival of TNBC cells, including MDA-MB-231, MDA-MB-436, MDA-MB-453, HCC-1937, 4T1, and BT20. These compounds also decreased the expression of Ki67 in these TNBC cells (Fig. 6A). In addition, treatment with a 20 μmol/L concentration of these compounds triggered ferroptosis in TNBC cells by increasing MDA levels, lipid peroxidation, and ROS levels in TNBC cells (Fig. 6B). Of these six compounds, compound 1 exhibited the strongest activity, while compound 5 had the weakest activity. These results confirm that Polygonum multiflorum Stilbene Glycoside Oligomers exert antitumor effects against TNBC cells.

Positive and negative controls in ferroptosis assays of TNBC cells

The above results revealed the factor that TSG induced the ferroptosis and inhibited the proliferation of TNBC cells. To further confirm the effect of TSG on TNBC cells, the experiments were conducted including the positive control sorafenib (Fig. 7A and B) and negative controls ferrostatin (Fig. 7C and D). As shown in Fig. 7, compared with the control group, treatment of sorafenib (10 μmol/L) and TSG (10 μmol/L) increased the lipid peroxidation levels in MDA-MB-231 cells, respectively (Fig. 7A and B). TSG showed higher efficiency

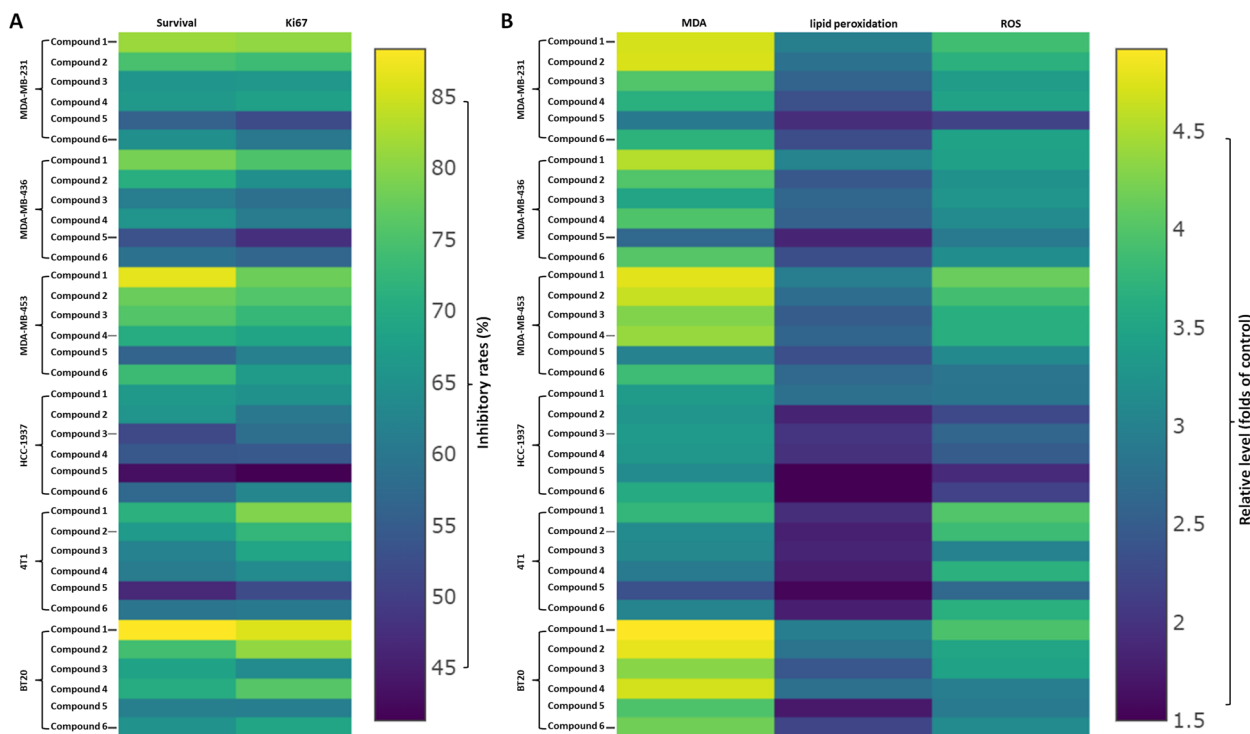


Fig. 6 The antitumor activation of Compounds on TNBC cells

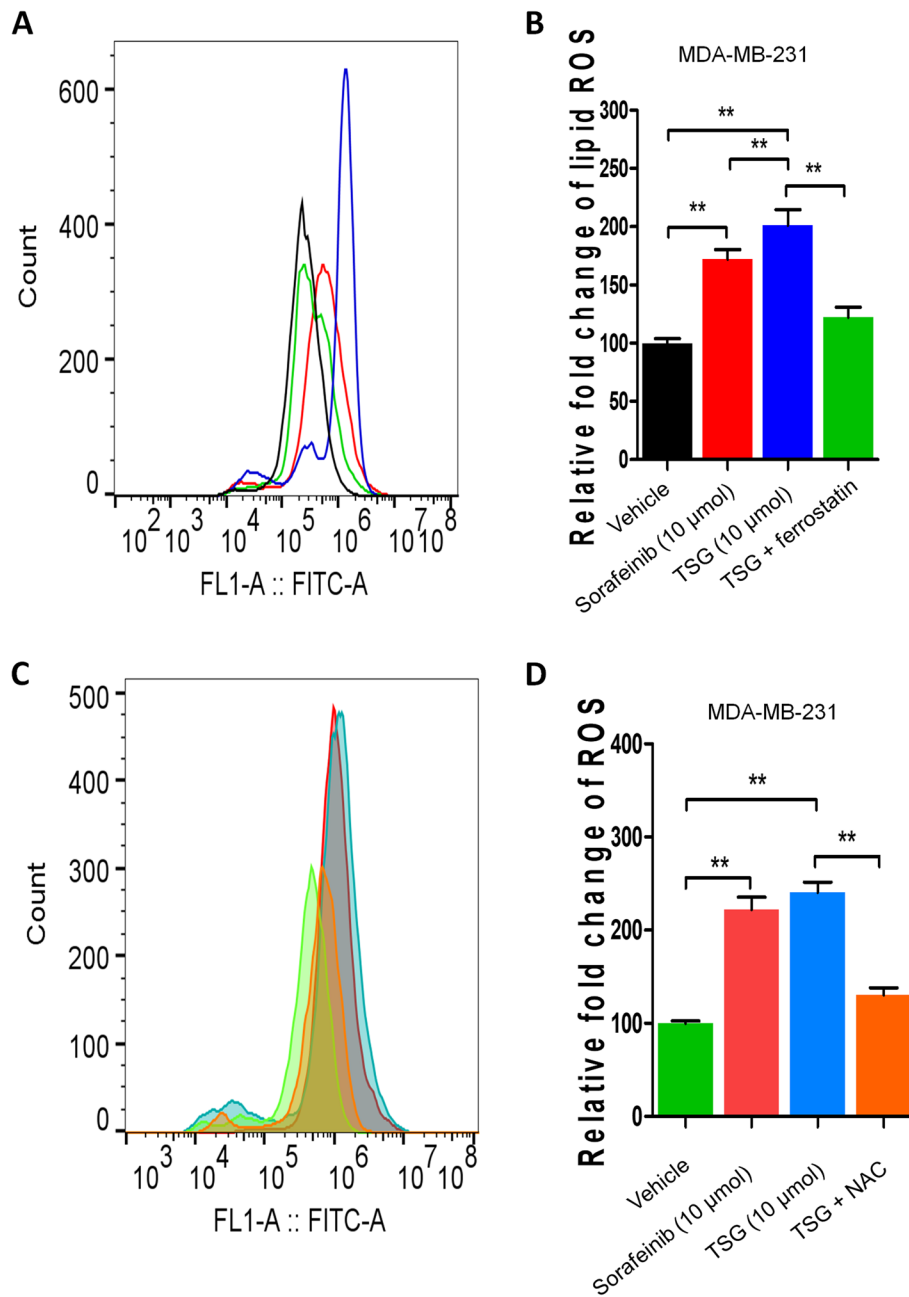


Fig. 7 The effect of TSG, Sorafenib or NAC on MDA-MB-231 cells' ferrostatin

compared with sorafenib (Fig. 7A and B). We also found that addition of ferrostatin (10 μmol/L) reversed the effect of TSG on promoted lipid peroxidation accumulation (Fig. 7C and D). These data demonstrated that TSG induced the ferroptosis in MDA-MB-231 cells.

The effect of TSG on P53/P21/SLC7A related mechanisms

As shown in Supplemental Fig. 1, the results indicated that TSG increased the level of p53 and p21, while reduced the level of SLC7A1 or GPX4 in MDA-MB-436 cells. These data may reveal the clues of TSG's mechanism in TNBC.

TSG exert GSH-depleting effect in a dose-dependent manner

Effect of tSG on lipid peroxidation and antioxidant enzyme activity was also examined. The results in Supplemental Fig. 2 indicated that TSG exert GSH-depleting effect in a dose-dependent manner. Combined with the results that TSG reduced the level of GPX4 in a dose-dependent manner (Supplemental Figure S1). These data provided further insight into the mechanism by which TSG induces ferroptosis.

Discussion

Of the three types of breast cancer, treatment strategies for triple-negative breast cancer (TNBC) are the most limited and patient prognosis remains unsatisfactory [15]. In recent years, TNBC has been considered to have heterogeneity and requires further subdivision, while related diagnostic and therapeutic research has also made continuous progress [16]. To better understand and treat TNBC, it can be divided into different types based on tissue features such as adenoid cystic carcinoma (ACC), poorly differentiated squamous cell carcinoma (NSC), fibroid tumor, and secretory triple negative breast cancer [17, 18]. Additionally, genotyping can also be used to distinguish TNBC, using various molecular markers such as keratin, EGFR, and laminin. Further subdivision of TNBC includes basal like (BL1 and BL2) TNBC, immunomodulatory (IM) TNBC, mesenchymal (M)-like TNBC, mesenchymal stem-like (MSL) TNBC, and luminal androgen receptor (LAR)-type TNBC [19, 20]. The traditional therapeutic strategies for TNBC are chemotherapy and neoadjuvant chemotherapy [21]. However, the sensitivity of different subtypes to these treatments varies. In addition to chemotherapy, there are other treatment strategies that are effective only for specific types of TNBC. For instance, olaparib is only effective against TNBC with embryonic BRCA mutations, and some immune checkpoint inhibitors can be used for the treatment of IM type TNBC [22]. This makes it essential to develop a broad-spectrum treatment strategy that works for all types of TNBC. In this study, active monomers of *Polygonum multiflorum*, represented by TSG, showed clear anti-tumor activity against various TNBC cells. Ferroptosis is considered a type of progressive cell death associated with cellular metabolism. Its primary feature is the lethal accumulation of lipid peroxides linked to numerous cellular physical processes related signaling pathways (e.g., lipid metabolism and redox homeostasis). Increasing evidence has revealed the roles of ferroptosis in human neurodegenerative diseases, infectious, inflammatory diseases, and malignancies [23, 24]. Interestingly, TNBC cells have a unique metabolic state (the iron and GSH homeostasis as the biochemical characteristics

including the accumulation of intracellular iron ions or lipid peroxides in TNBC cells) that makes them potentially sensitive to ferroptosis [11]. Recently, inducing ferroptosis in tumor cells has become a potential strategy for cancer therapy by modulating various tumor properties. Agents such as sulfasalazine, erastin, or RSL3 have been used as antitumor drugs by inducing cellular ferroptosis, which can also reduce cancer growth and resistance [11]. Our results not only extended the knowledge of ferroptosis in TNBC, but also will provided novel approach for TNNBC based on TSG and *Polygonum multiflorum*.

TSG (C₂₀H₂₂O₉) is a unique active ingredient discovered and extracted from PM in 1975, with various pharmacological properties through modulating multiple signaling transduction pathways such as NF-κB, PI3K-AKT, ERK1/2, AMPK, Nrf2, Bcl-2/Bax/Caspase-3, ROS-NO, TGFβ/Smad, MAPK, and SIRT1 [1–5]. Although diverse studies are conducted with renal and cardiovascular pathologies, these signaling pathways visualize the molecular mechanisms of compounds such as TSG. They are closely related to malignancy development, progression, metastasis, invasion, or resistance to anti-tumor therapeutic strategies, making it essential to investigate the role of TSG in cancer. Among these pathways, PI3K-AKT, ERK1/2, and MAPK are positive regulators of cancerous cells, closely related to poor patient prognosis [25, 26]. The NF-κB pathway and Bcl-2/Bax/Caspase-3 are key regulatory mechanisms for cellular pro-survival and anti-apoptosis, crucial in anti-tumor therapy resistance [27, 28]. Additionally, TGFβ/Smads pathway is capable of inducing cellular epithelial mesenchymal transition, closely related to fibrosis [29, 30]. In this study, we reported the antitumor activity of TSG on TNBC cells and specifically investigated the induction of ferroptosis in these cells by TSG. The molecular mechanism underlying TSG-induced ferroptosis in TNBC cells is not clear and will be further explored in future studies. Starting from the existing known possible signaling pathways of TSG is a feasible approach. Among these pathways, PI3K/AKT, ERK1/2, MAPK, NF-κB, TGFβ/Smads have all been reported to be associated with ferroptosis [31–34]. It is of great significance to use inhibitors of these pathways (such as LY294002, PD98059, SB431542, BIBR796, and ZLDI8) to detect which signaling pathway TSG may induce TNBC ferroptosis [35–40]. It is worth mentioning that sorafenib is considered a positive drug for inducing ferroptosis, and its mechanism of action is to inhibit the activity of a series of receptor tyrosine protein kinases, as well as the activity of downstream PI3K/AKT and MAPK pathways [41, 42]. This provides a reference for TSG related research.

Although TSG is a typical and important hesperidin analogue, this study used six different hesperidin

analogues in total. The chemical structure nucleus shared by all these compounds features glutamic acid as the core component; each compound's unique substituents are added to this nucleus [1–5]. Compound 1 consists of two glutamic acids, while Compound 2 adds an acetyl group on top of glutamic acid. Compound 3 is simply a single glutamic acid, whereas Compound 4 (TSG) features the addition of an extra hydrogen atom to glutamic acid. Compound 5 includes both methoxy and methyl groups along with glutamic acid. Lastly, Compound 6 comprises simply glutamic acid plus two additional hydrogen atoms. We tested the anti-tumor activity of each compound at a dose of 20 micromoles per liter on various TNBC cells, assessing indicators such as cell survival and Ki67 expression. Additionally, ferroptosis was also examined using this detection method. This panel can intuitively reflect the overall activity of each compound, allowing for some comparisons between them. Compound 1 showed higher overall activity than the remaining five compounds, whereas Compound 5 exhibited the weakest activity. We inferred that more hydroxyl groups substituted on the parent nucleus contribute to enhanced activity among these compounds. However, methyl or methoxy groups can also impact the activity of these compounds. Through structure–activity analysis, the hydrogen atom, ethylene double bond, and phenolic hydroxyl group with strong electrophilicity connected to the benzene ring are the main effector groups in the components of stilbene glycosides and their corresponding metabolites. Other substituents on the benzene ring determine the strength of the pharmacological effect of the component and give it some effect characteristics. In addition, most of the metabolites of stilbene glycosides retain the basic skeleton of the compound itself, which may result in a “superposition effect” between a component and its metabolite, that is, due to the fact that multiple chemical prototype components and metabolites may be isomers, they will produce an additive effect on the same target, equivalent to the “superposition effect of multiple component single targets”. Taking compound 3 as an example, the C5'-OH and C4'-OH groups on the benzene ring exhibit antioxidant activity, and the glucosidic bond at position 2 in the structure generates an electron donating effect, making the phenoxide formed by C5'-OH more stable and facilitating the termination of free radical chain reactions, enhancing antioxidant activity; However, C3'-OH has weaker antioxidant activity due to the steric hindrance effect of adjacent glycosides. Furthermore, stilbene glycosides belong to natural polyphenolic compounds, and their parent nucleus structure and the number and position of active hydroxyl groups can affect their affinity with metabolic enzymes, generating different types of metabolites through different metabolic pathways. The

substituents in the basic skeleton of this type of component also determine the type of metabolic reaction that occurs. For compound 3, the glucuronidation of the hydroxyl group on the benzene ring is the main metabolic reaction. Through metabolism, more polar groups can be introduced into the prototype drug, which can easily bind with endogenous components such as glucuronic acid, amino acids, and glutathione in the body, generating highly polar and water-soluble metabolites, and also increasing the activity of the prototype drug to a certain extent. Further research will be conducted in the future to delve deeper into their structure–activity relationships and identify optimal compound structures for anti-tumor activity.

Conclusion

In summary, the results in the presence work identified the activation that TSG induce the ferroptosis and inhibited the proliferation of TNBC cells. These provide a foundation for future research of TSG and TNBC treatment.

Abbreviations

TSG	Trans-2,3,5,4'-tetrahydroxystilbene 2-O-β-D-glucopyranoside
<i>P. multiflorum</i>	<i>Polygonum multiflorum</i> m Thunb
TNBC	Triple-negative breast cancer
MDA	Malondialdehyde
4-HNE	4-Hydroxynonenal
ROS	Reactive oxygen species
H&E	Hematoxylin and eosin
Ki67	An indicator of cell proliferation
IM	Immunomodulatory

Supplementary Information

The online version contains supplementary material available at <https://doi.org/10.1186/s12885-025-13999-z>.

Supplementary Material 1: Supplemental Figure 1. TSG modulates the expression of P53 pathway related factors in MDA-MB-436 cells.

Supplementary Material 2: Supplemental Figure 2. TSG exert GSH-depleting effect in a dose-dependent manner.

Supplementary Material 3: Supplemental Figure 3.

Acknowledgements

We deeply appreciate the help and advice from Prof. Yingshi Zhang at Shenyang Pharmaceutical University.

Authors' contributions

XML: Writing—original draft, Supervision, Methodology, Investigation, Conceptualization. HY: Visualization, Investigation. TTC: Visualization, Investigation. ZSY: Visualization, Investigation. HJ: Supervision, Writing—review & editing. SYN: Funding acquisition, Supervision, Writing—review & editing.

Funding

This work is supported by the Medical Science Foundation of Hebei University (Approval ID: 2024B08) from the Chinese Government.

Data availability

Data is provided within the manuscript.

Declarations

Ethics approval and consent to participate

The Animal Ethics Committee of the Affiliated Hospital of Hebei University reviewed and approved the breeding and use of experimental animals, as well as the experimental designs and methods (Approval ID: IACUC-2021XG020). All animal experiments were performed in accordance with the UK Animals (Scientific Procedures) Act of 1986 and associated guidelines.

Consent for publication

Not applicable.

Competing interests

The authors declare no competing interests.

Author details

¹School of Clinical Medicine, Hebei University, Baoding 071000, China. ²Department of Breast Surgery, Affiliated Hospital of Hebei University, Baoding 071000, China. ³Department of Medical Oncology - Hebei Key Laboratory of Cancer Radiotherapy and Chemotherapy, Affiliated Hospital of Hebei University, Baoding 071000, China. ⁴Department of Clinical Laboratory, Affiliated Hospital of Hebei University, Baoding 071000, China. ⁵Department of Histology and Embryology, School of Basic Medical Sciences, Hebei University, Baoding 071000, China. ⁶School of Traditional Chinese Medicine, Shenyang Medical College, Shenyang 110034, China.

Received: 10 October 2024 Accepted: 24 March 2025

Published online: 14 April 2025

References

- Wang C, Dai S, Gong L, et al. A Review of Pharmacology, Toxicity and Pharmacokinetics of 2,3,5,4'-Tetrahydroxystilbene-2-O- β -D-Glucoside. *Front Pharmacol.* 2022;12:791214.
- Liu Y, Wang Q, Yang J, et al. Polygonum multiflorum Thunb.: A Review on Chemical Analysis, Processing Mechanism, Quality Evaluation, and Hepatotoxicity. *Front Pharmacol.* 2018;9:364.
- Teka T, Wang L, Gao J, et al. Polygonum multiflorum: Recent updates on newly isolated compounds, potential hepatotoxic compounds and their mechanisms. *J Ethnopharmacol.* 2021;271:113864.
- Li S, Huang X, Zhong Y, et al. Stilbene Glycoside Oligomers from the Roots of Polygonum multiflorum. *Chem Biodivers.* 2019;16(6):e1900192.
- Rao T, Liu Y, Zeeng X, et al. The hepatotoxicity of Polygonum multiflorum: The emerging role of the immune-mediated liver injury. *Acta Pharmacol Sin.* 2021;42(1):27–35.
- Gay Y, Li J, Li J, et al. Tetrahydroxy stilbene glycoside alleviated inflammatory damage by mitophagy via AMPK related PINK1/Parkin signaling pathway. *Biochem Pharmacol.* 2020;177:113997.
- Wang S, Wang Y, Wang Y, et al. Myc derived circRNA promotes triple-negative breast cancer progression via reprogramming fatty acid metabolism. *Discov Oncol.* 2023;14(1):67.
- Dri A, Arpino G, Bianchini G, et al. Breaking barriers in triple negative breast cancer (TNBC) - Unleashing the power of antibody-drug conjugates (ADCs). *Cancer Treat Rev.* 2024;123:102672.
- Yang H, Ren L, Wang Y, et al. FBI-1 enhanced the resistance of triple-negative breast cancer cells to chemotherapeutic agents via the miR-30c/PXR axis. *Cell Death Dis.* 2020;11(10):851.
- Hao J, Chen Q, Feng Y, et al. Combination treatment with FAAH inhibitors/URB597 and ferroptosis inducers significantly decreases the growth and metastasis of renal cell carcinoma cells via the PI3K-AKT signaling pathway. *Cell Death Dis.* 2023;14(4):247.
- Li P, Lin Q, Sun S, et al. Inhibition of cannabinoid receptor type 1 sensitizes triple-negative breast cancer cells to ferroptosis via regulating fatty acid metabolism. *Cell Death Dis.* 2022;13(9):808.
- Liu M, Xu C, Yang H, et al. Pro-oncogene FBI-1 inhibits the ferroptosis of prostate carcinoma PC-3 cells via the microRNA-324-3p/GPX4 axis. *J Cancer.* 2024;15(13):4097–112.
- Zhang Y, Li D, Jiang Q, et al. Novel ADAM-17 inhibitor ZLDI-8 enhances the in vitro and in vivo chemotherapeutic effects of Sorafenib on hepatocellular carcinoma cells. *Cell Death Dis.* 2018;9(7):743.
- Sun J, Chang Z, Gao X, et al. Novel nanoparticle CS-C60-Fe3O4 magnetically induces tissue-specific aggregation and enhances thermal ablation of hepatocellular carcinoma. *Cancer Nanotechnol.* 2024;15(8):1–16.
- Shi Z, Liu Y, Zhang S, et al. Evaluation of predictive and prognostic value of androgen receptor expression in breast cancer subtypes treated with neoadjuvant chemotherapy. *Discov Oncol.* 2023;14(1):49.
- Harris MA, Savas P, Virassamy B, O'Malley MMR, Kay J, Mueller SN, Mackay LK, Salgado R, Loi S. Towards targeting the breast cancer immune micro-environment. *Nat Rev Cancer.* 2024;24(8):554–77. <https://doi.org/10.1038/s41568-024-00714-6>.
- Che J, Chen B, Wang X, et al. Correlation analysis of DLG5 and PD-L1 expression in triple-negative breast cancer. *BMC Cancer.* 2025;25(1):35.
- Chakraborty M, Kaur J, Gun J, et al. Clinical relevance of glycosylation in triple negative breast cancer: a review. *Glycoconj J.* 2024;41(2):79–91.
- Pastena P, Perera H, Martinino A, et al. Unraveling Biomarker Signatures in Triple-Negative Breast Cancer: A Systematic Review for Targeted Approaches. *Int J Mol Sci.* 2024;25(5):2559.
- Dhanushkumar T, Selvam PK, Rambabu M, et al. Advancements and hurdles in the development of a vaccine for triple-negative breast cancer: A comprehensive review of multi-omics and immunomics strategies. *Life Sci.* 2024;337:122360.
- Xiong N, Wu H, Yu Z. Advancements and challenges in triple-negative breast cancer: a comprehensive review of therapeutic and diagnostic strategies. *Front Oncol.* 2024;14:1405491.
- Ou Y, Wang M, Xu Q, et al. Small molecule agents for triple negative breast cancer: Current status and future prospects. *Transl Oncol.* 2024;41:101893.
- Jiang X, Stockwell BR, Conrad M. Ferroptosis: mechanisms, biology and role in disease. *Nat Rev Mol Cell Biol.* 2021;22(4):266–82.
- Tang D, Chen X, Kang R, et al. Ferroptosis: molecular mechanisms and health implications. *Cell Res.* 2021;31(2):107–25.
- Zhao Q, Yu M, Li J, et al. GLUT1 inhibits hepatocellular carcinoma progression via ROS-mediated p38/JNK MAPK pathway activation and mitochondrial apoptosis. *Discov Oncol.* 2024;15(1):8.
- Wang G, Zhang X, Zhou Z, et al. Sphingosine 1-phosphate receptor 2 promotes the onset and progression of non-alcoholic fatty liver disease-related hepatocellular carcinoma through the PI3K/AKT/mTOR pathway. *Discov Oncol.* 2023;14(1):4.
- Giuli MV, Mancusi A, Giuliani E, et al. Notch signaling in female cancers: a multifaceted node to overcome drug resistance. *Cancer Drug Resist.* 2021;4(4):805–36.
- Jia H, Wang Z, Zhang J, et al. γ -Secretase inhibitors for breast cancer and hepatocellular carcinoma: From mechanism to treatment. *Life Sci.* 2021;268:119007.
- Saitoh M. Transcriptional regulation of EMT transcription factors in cancer. *Semin Cancer Biol.* 2023;97:21–9.
- Wang X, Eichhorn P, Thiery JP. TGF- β , EMT, and resistance to anti-cancer treatment. *Semin Cancer Biol.* 2023;97:1–11.
- Huang X, Xia K, Wei Z, et al. SLC38A5 suppresses ferroptosis through glutamine-mediated activation of the PI3K/AKT/mTOR signaling in osteosarcoma. *J Transl Med.* 2024;22(1):1004.
- Xie Y, Yu H, Ye Y, Wang J, Yang Z, Zhou E. Activation of Ferroptosis and NF- κ B/NLRP3/MAPK Pathways in Methylmercury-Induced Hepatotoxicity. *Toxicol Ind Health.* 2025;41(3):131–9. <https://doi.org/10.1177/07482337241307067>.
- Liu R, Wang Z, Luo Q, et al. Hot air injures human alveolar epithelial cells through ERK1/2 signaling-mediated ferroptosis. *J Therm Biol.* 2025;127:104065.
- Yuan Y, Wang Y, Yan Y, et al. FBLN1 regulates ferroptosis in acute respiratory distress syndrome by reducing free ferrous iron by inhibiting the TGF- β /Smad pathway. *PLoS ONE.* 2024;19(12):e0314750.
- Hu J, Dai C, Ding Z, et al. IKBIP promotes tumor development via the akt signaling pathway in esophageal squamous cell carcinoma. *BMC Cancer.* 2024;24(1):759.
- Zuchegna C, Leone S, Romano A, et al. KRAS is a molecular determinant of platinum responsiveness in glioblastoma. *BMC Cancer.* 2024;24(1):77.
- Wible D, Parikh Z, Cho EJ, et al. Unexpected inhibition of the lipid kinase PIKfyve reveals an epistatic role for p38 MAPKs in endolysosomal fission and volume control. *Cell Death Dis.* 2024;15(1):80.

38. Zhou H, Liu M, Deng T, et al. The TGF- β /Smad Pathway Inhibitor SB431542 Enhances The Antitumor Effect Of Radiofrequency Ablation On Bladder Cancer Cells. *Onco Targets Ther.* 2019;12:7809–21.
39. Xu C, Gao X, Ren T, et al. The ADAM17 inhibitor ZLDI-8 sensitized hepatocellular carcinoma cells to sorafenib through Notch1-integrin β -talk. *Pharmacol Res.* 2024;203:107142.
40. Lu H, Wu C, Jiang XW. ZLDI-8 suppresses angiogenesis and vasculogenic mimicry in drug-resistant NSCLC in vitro and in vivo. *Lung Cancer.* 2023;182:107279.
41. Cao J, Zhou T, Wu T, et al. Targeting estrogen-regulated system x(c)⁻ promotes ferroptosis and endocrine sensitivity of ER⁺ breast cancer. *Cell Death Dis.* 2025;16(1):30.
42. Liu R, Cui H, Li D, et al. Roles and Mechanisms of Ferroptosis in Sorafenib Resistance for Hepatocellular Carcinoma. *J Hepatocell Carcinoma.* 2024;11:2493–504.

Publisher's Note

Springer Nature remains neutral with regard to jurisdictional claims in published maps and institutional affiliations.